

# MULTI-LOCATION WIDEBAND THROUGH-THE-WALL BEAMFORMING

Fauzia Ahmad

Radar Imaging Lab, Center for Advanced Communications, Villanova University  
800 Lancaster Ave, Villanova, PA 19085, USA  
E-mail: fauzia.ahmad@villanova.edu

## ABSTRACT

*Significant multipath propagation and heavy clutter in indoor environments renders through-the-wall radar imaging a difficult and complex proposition. It is highly desirable to properly interpret the radar images and determine the contents of the indoor scene with a high level of confidence. Data collected from multiple positions around a structure can be used to improve imaging visibility into the indoor scene, thereby enhancing indoor target detection and localization. In this paper, we consider multi-location radar imaging. Image fusion techniques for combining radar images acquired from multiple locations along two sides of an enclosed structure are presented. Supporting results, based on real-data, are also provided.*

**Index Terms**— Through-the-wall, radar imaging, array signal processing, synthetic aperture radar, image fusion.

## 1. INTRODUCTION

Sensing through obstacles, such as walls and doors, using microwave signals is emerging as a powerful tool supporting a range of civilian and military applications [1-2]. Compared to other radar applications, through-the-wall radar imaging (TWRI) is a complex and difficult problem that faces many challenges. Ambiguities and inaccuracies in wall parameters, and presence of non-uniform walls, multiple walls, and operator motion can severely degrade system performance. It is highly desirable to detect, locate, and classify a variety of indoor targets, both moving and stationary, enclosed in small spaces and in the presence of significant multipath propagation and heavy clutter.

Given the vagaries of TWRI, it is important to interpret the radar images and determine the contents of the indoor scene with a high level of fidelity. Image enhancement techniques, such as nonlinear filtering, can be used to improve the signal-to-clutter ratio, thereby improving image quality and target location accuracy. In many situations, access is available to multiple locations along one exterior wall and/or to more than one side of the enclosed structure under consideration. We refer to these situations as multi-location imaging. Multi-location radar imaging improves

the accuracy of target localization and identification by reducing false alarms due to secondary reflections.

In this paper, we present strategies for integration of images acquired from various positions along two sides of a building. These images are obtained using wideband beamforming that incorporates the effects of signal propagation through the wall. Since the images obtained from different positions around the building have different coordinate systems, image integration consists of image registration followed by fusion. Registration transforms the sets of images into a single coordinate system. Fusion can then take place to generate a composite through-the-wall image that provides enhanced scene interpretation.

## 2. WIDEBAND THROUGH-THE-WALL BEAMFORMING

We present the fundamental equations describing wideband beamforming in the presence of a uniform wall [3]. Consider an  $M$ -element 2-D array of transceivers, located parallel to the  $xy$ -plane at a standoff distance  $z_{off}$  from a wall of thickness  $d$  and dielectric constant  $\epsilon$ , as shown in Fig. 1(a). The region being imaged is located beyond the wall along the positive  $z$ -axis. Let the  $m$ -th transceiver, located at  $\mathbf{x}_{im} = (x_{im}, y_{im}, -z_{off})$ , illuminate the scene with a stepped-frequency CW signal composed of  $K$  components. The complex amplitude of the returns, at each frequency, is measured at the same transceiver location only. For a single point target located at  $\mathbf{x}_p = (x_p, y_p, z_p)$ , the complex amplitude,  $r_{mk}$ , corresponding to the  $k$ -th frequency,  $\omega_{mk}$ , measured at the  $m$ -th transceiver is given by  $a(\mathbf{x}_p)\exp(-j\omega_k\tau_{mp})$ , where  $a(\mathbf{x}_p)$  is the complex reflectivity of the point target and  $\tau_{mp}$  is the two-way signal propagation delay given by [3]

$$\tau_{mp} = 2(l_{mp,air,1} + \sqrt{\epsilon}l_{mp,wall} + l_{mp,air,2}) / c \quad (1)$$

Here,  $c$  is the speed of light. The variables  $l_{mp,air,1}$ ,  $l_{mp,wall}$ , and  $l_{mp,air,2}$  represent the traveling distances of the signal before, through, and beyond the wall,

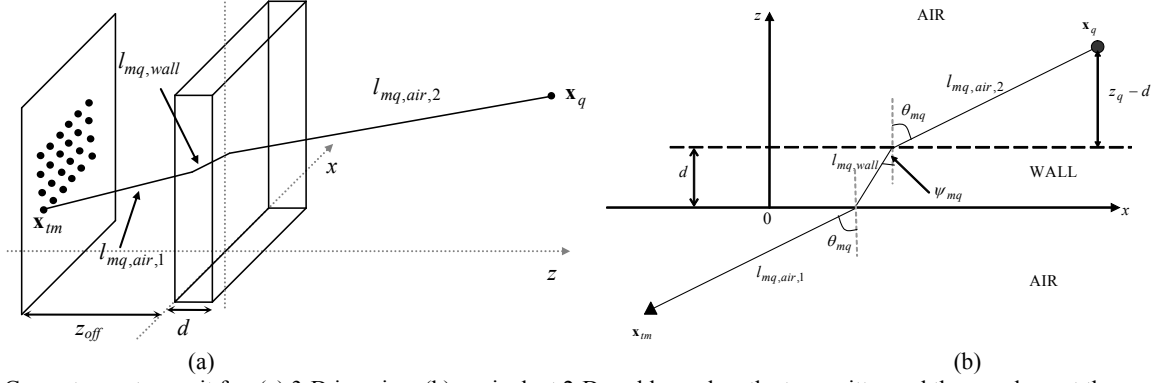


Fig. 1. Geometry on transmit for (a) 3-D imaging, (b) equivalent 2-D problem when the transmitter and the voxel are at the same height.

respectively, from the  $m$ -th transceiver to the target at  $\mathbf{x}_p$ . This process is repeated at each transceiver location until all  $M$  locations have been exhausted. The region of interest is, then, divided into a finite number of volume pixels (voxels) in downrange, crossrange, and height, represented by the  $z$ ,  $x$ , and  $y$  coordinates, respectively. For the  $q$ -th image voxel located at  $\mathbf{x}_q = (x_q, y_q, z_q)$ , phase delays, corresponding to each frequency and determined by the propagation path from each transceiver to  $\mathbf{x}_q$ , are applied to the  $M$  received signals. The corresponding complex amplitude voxel value,  $I(\mathbf{x}_q)$ , is then obtained by [3]

$$I(\mathbf{x}_q) = \sum_{k=1}^K \sum_{m=1}^M a(\mathbf{x}_p) \exp(-j\omega_k(\tau_{mp} - \tau_{mq})) \quad (2)$$

Here,  $\tau_{mq}$  is the focusing delay, which is given by (1) with the target voxel subscript  $p$  replaced by the focusing voxel subscript  $q$ . The process described by (2) is performed for all voxels in the region of interest to generate the composite image of the scene. The general case of multiple targets can be obtained by superposition of target reflections.

In order to compute the focusing delay, consider the traveling from the  $m$ -th transceiver at  $\mathbf{x}_{tm}$  to the  $q$ -th voxel at  $\mathbf{x}_q$ , as shown in Fig. 1. If both  $\mathbf{x}_{tm}$  and  $\mathbf{x}_q$  are at the same height, then the problem reduces to the equivalent 2-D problem, shown in Fig. 1(b). In this case,  $l_{mp,air,1}$ ,  $l_{mp,wall}$ , and  $l_{mp,air,2}$  are given by [3]

$$l_{mp,air,1} = \frac{z_{off}}{\cos\theta_{mq}}, \quad l_{mp,wall} = \frac{d}{\cos\psi_{mq}}, \quad l_{mp,air,2} = \frac{z_q - d}{\cos\theta_{mq}} \quad (3)$$

where  $\theta_{mq}$  is the incident angle, and  $\psi_{mq}$  is the angle of refraction, which can be computed by solving

$$\begin{aligned} & (x_q - (x_{tm} + z_{off} \tan\theta_{mq}))^2 + z_q^2 \\ &= l_{mq,wall}^2 + l_{mq,air,2}^2 + 2l_{mq,wall}l_{mq,air,2} \cos(\psi_{mq} - \theta_{mq}) \quad (4) \\ & \phi_{mp} = \sin^{-1}(\sin(\theta_{mq}) / \sqrt{\epsilon}) \end{aligned}$$

If  $\mathbf{x}_{tm}$  and  $\mathbf{x}_q$  assume different heights, a rotation transform

is applied so that in the new coordinate system, the  $m$ -th transceiver and the  $q$ -th voxel are at the same height [4], i.e.,

$$\begin{bmatrix} x'_{tm} \\ y'_{tm} \end{bmatrix} = \begin{bmatrix} \cos\beta & \sin\beta \\ -\sin\beta & \cos\beta \end{bmatrix} \begin{bmatrix} x_{tm} \\ y_{tm} \end{bmatrix}, \quad \begin{bmatrix} x'_q \\ y'_q \end{bmatrix} = \begin{bmatrix} \cos\beta & \sin\beta \\ -\sin\beta & \cos\beta \end{bmatrix} \begin{bmatrix} x_q \\ y_q \end{bmatrix} \quad (5)$$

such that  $y'_{tm} = y'_q$ . This implies that

$$\tan\beta = (y_{tm} - y_q) / (x_{tm} - x_q) \quad (6)$$

Eqs. (3)-(4) can then be used to compute the traveling distances with  $x_{tm}$  and  $x_q$ , respectively, replaced by  $x'_{tm} = \cos\beta x_{tm} + \sin\beta y_{tm}$  and  $x'_q = \cos\beta x_q + \sin\beta y_q$ .

### 3. MULTI-LOCATION IMAGING

Data collected from multiple locations around the structure can be used to improve visibility into the indoor scene being imaged. Below, we present techniques for integration of images obtained from  $N$  vantage points along the front and one side of a structure. It is assumed that the interior layout, the relative locations and the standoff distances of the imaging radar are exactly known. For the first imaging position along the front wall, the  $xyz$ -coordinate system, as defined in Fig. 2, is used. This coordinate system will serve as the reference for image registration. The indoor region being imaged is bounded by  $[x_{min}, x_{max}]$ ,  $[y_{min}, y_{max}]$ , and  $[z_{min}, z_{max}]$  along the  $x$ ,  $y$ , and  $z$  axes, respectively, and is divided into  $Q$  voxels. Let  $\{I_1(\mathbf{x}_q)\}_{q=1}^Q$  be the corresponding complex amplitude beamformed image. Let  $\tilde{x}\tilde{y}\tilde{z}$  be the sensor specific coordinate system for the  $n$ -th vantage point ( $n > 1$ ), defined in Figs. 2(a) and (b), respectively, for imaging from the  $n$ -th position along the front and the side wall. The bounds on the same indoor region in either case are denoted by  $[\tilde{x}_{min}, \tilde{x}_{max}]$ ,  $[\tilde{y}_{min}, \tilde{y}_{max}]$ , and  $[\tilde{z}_{min}, \tilde{z}_{max}]$  along the respective axes. For the vantage point along the front wall, the  $\tilde{x}\tilde{y}\tilde{z}$ -coordinate system is a simple translation of the  $xyz$ -axes (See Fig. 2(a)),

$$\tilde{x} = x - x_0, \quad \tilde{y} = y, \quad \tilde{z} = z \quad (7)$$

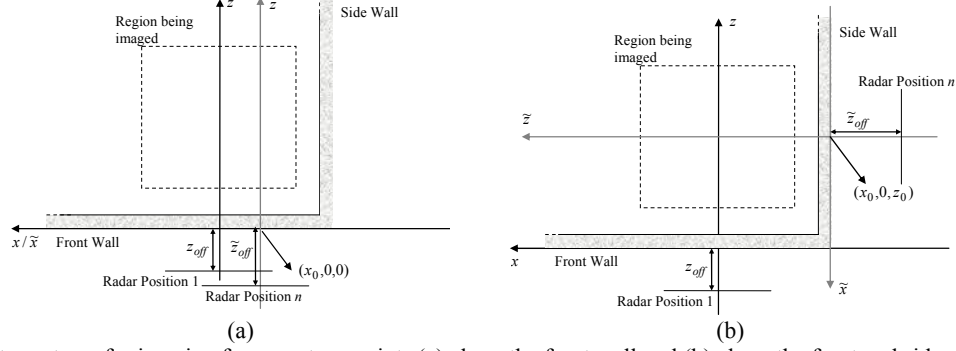


Fig. 2. Coordinate systems for imaging from vantage points (a) along the front wall and (b) along the front and side walls of a structure.

where  $x_0$  is the translation value. On the other hand, the  $\tilde{x}\tilde{y}\tilde{z}$ -coordinate system for the location along the side wall is a rotation and translation of the  $xyz$ -axes (See Fig. 2(b)),

$$\begin{bmatrix} \tilde{x} \\ \tilde{y} \\ \tilde{z} \end{bmatrix} = \begin{bmatrix} \cos \xi & 0 & -\sin \xi \\ 0 & 1 & 0 \\ \sin \xi & 0 & \cos \xi \end{bmatrix} \begin{bmatrix} x - x_0 \\ y \\ z - z_0 \end{bmatrix} \quad (8)$$

where  $[x_0 \ 0 \ z_0]^T$  are the translation values and  $\xi$  is the counter-clockwise rotation angle, which equals  $90^\circ$  in this case. If access is available to the back wall instead,  $\xi$  equals  $180^\circ$ . For comparability, the voxel sampling grids for the  $n$ -th location ( $n > 1$ ) and the first vantage point are chosen to be identical. In general, a different voxel sampling grid can be used, but then the registration process requires interpolation to align the  $N$  images. Let  $\{\tilde{I}_n(\tilde{\mathbf{x}}_q)\}_{q=1}^Q$  be the image, acquired from the  $n$ -th position ( $n > 1$ ) with array locations  $\{\tilde{\mathbf{x}}_{im} = (\tilde{x}_{im}, \tilde{y}_{im}, -\tilde{z}_{off})\}_{m=1}^M$ . With  $xyz$ -coordinates as the reference, the registration process is simply an identity mapping from the image  $\{\tilde{I}_n(\tilde{\mathbf{x}}_q)\}_{q=1}^Q$  to a corresponding image  $\{I_n(\mathbf{x}_q)\}_{q=1}^Q$  where  $\tilde{\mathbf{x}}_q$  and  $\mathbf{x}_q$  are related by transformation (7) or (8).

### 3.1. Fusion of Imaging Results

For the general problem of enhanced target detection in multi-aspect or multi-location radar imaging, traditional statistical detection schemes have been adapted for image fusion under the assumption of Gaussian distributed clutter and noise [4]. Since the indoor clutter characteristics are quite different from those reported in other contexts, the Gaussian model is hardly valid for TWRI. We, therefore, resort to a simple fusion technique based on direct thresholding, which is described below. Detailed analysis, along with an alternate fusion scheme, can be found in [5].

Let the  $n$ -th normalized magnitude image,  $\{P_n(\mathbf{x}_q)\}_{q=1}^Q$ , be defined as

$$P_n(\mathbf{x}_q) = |I_n(\mathbf{x}_q)| / \max(\{|I_n(\mathbf{x}_q)|\}_{q=1}^Q), \quad n = 1, 2, \dots, N \quad (9)$$

For a given voxel  $\mathbf{x}_q$ , a binary detection problem can be defined by hypotheses  $H_1$  and  $H_0$ , where  $H_1$  is defined as the target being present, and  $H_0$  is defined as ‘no target’ at  $\mathbf{x}_q$ . For TWRI applications, detection and localization of specific targets, such as human beings and cache of weapons, is of particular interest. As such, the radar cross-section (RCS) of the targets of interest can be used to set the threshold so that the return from the weakest target, located farthest from the radar, will result in the target being detected. This detection scheme is individually applied to each of the  $N$  images. The resulting output, corresponding to the image  $\{P_n(\mathbf{x}_q)\}_{q=1}^Q$ , is a binary image,  $\{B_n(\mathbf{x}_q)\}_{q=1}^Q$ , with its  $q$ -th voxel defined as

$$B_n(\mathbf{x}_q) = \begin{cases} 1 & \text{if } P_n(\mathbf{x}_q) \geq \beta \quad (H_1 \text{ is true}) \\ 0 & \text{if } P_n(\mathbf{x}_q) < \beta \quad (H_0 \text{ is true}) \end{cases} \quad (10)$$

where  $\beta$  is the RCS-based threshold value. The  $N$  binary images can be fused in one of the following ways. For a given voxel  $\mathbf{x}_q$ , a ‘target is present’ decision is made if

(i)  $B_n(\mathbf{x}_q) = 1 \ \forall n$ , i.e.,

$$B_{final}(\mathbf{x}_q) = \prod_{n=1}^N B_n(\mathbf{x}_q) \quad (11)$$

where  $\{B_{final}(\mathbf{x}_q)\}_{q=1}^Q$  is the fused binary image.

(ii)  $B_n(\mathbf{x}_q) = 1$  for at least ‘ $L$  out of  $N$ ’ ( $L \neq N$ ) images, i.e.

$$B_{final}(\mathbf{x}_q) = \begin{cases} 1 & \text{if } \sum_{n=1}^N B_n(\mathbf{x}_q) \geq L \\ 0 & \text{otherwise} \end{cases} \quad (12)$$

The second scheme is particularly useful for cases where a target is not visible from all positions around the building.

## 4. EXPERIMENTAL RESULTS

A wideband synthetic aperture through-the-wall radar system was set up in the Radar Imaging Lab at Villanova University. An Agilent network analyzer, ENA 5071B, was used to synthesize a stepped-frequency CW signal, consisting of 801 frequency steps, covering 0.7-3.1GHz. A

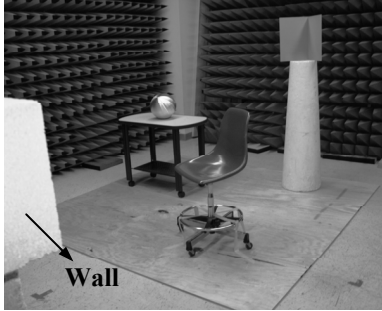


Fig. 3. Indoor scene being imaged

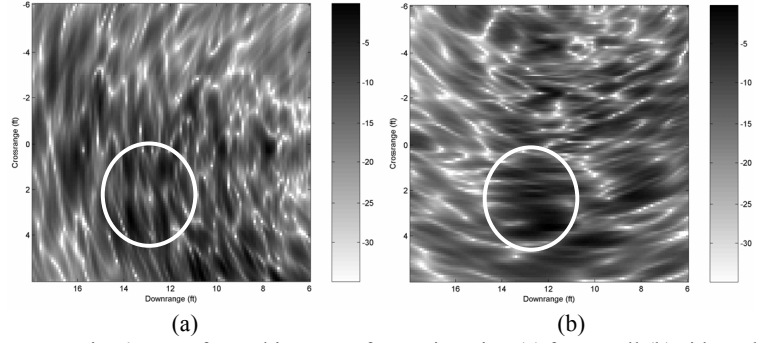


Fig. 4. Beamformed images, after registration (a) front wall (b) side wall

horn antenna with 0.7-6GHz operational bandwidth, was used as the transceiver and mounted on a 2-D scanner to synthesize a 57x57 element square array with 0.875in inter-element spacing. A 10ft x 8ft solid concrete block wall, with  $d=5.625\text{in}$  and  $\epsilon=7.66$ , was positioned 40in downrange from the antenna feed. A dihedral, a 10in diameter sphere, a 27.5in high table with metal legs, and a chair with seat height of 21in were mounted on a turntable made of two 4ft x 8ft sheets of plywood. Data was collected first with the setting of Fig. 3 and then with the turntable rotated clockwise by  $90^\circ$  so as to emulate imaging from the side wall. Empty scene measurements were also made with only the turntable present for coherent background subtraction.

B-scan images (downrange vs. crossrange horizontal cuts through the 3D volume) of a 12ft x 12ft region, centered at (0in, 27.5in, 8ft 8in) in the  $xyz$ -coordinates, corresponding to the two vantage points, were obtained using the through-the-wall beamformer of Section 2 and are shown, after registration, in Fig. 4. The height of the B-scan images corresponds to the height of the table. In both Figs. 4(a) and (b), the returns from the table, in particular the metal legs of the table, are visible at the correct locations. However, both images contain several false targets of strengths comparable to the target of interest, resulting from multipath and target interactions. Without any a priori knowledge, it is difficult to discern the target presence in either image. Figs. 5(a) and (b) show the corresponding binary images. Since the RCS of the table was unavailable, we set the threshold so that all returns within 5dB of the strongest return would qualify as a target. The fused binary image, based on eq. (11), is shown in Fig. 5(c). We observe that the fused image has localized the target of interest with the least number of false targets present.

## 6. CONCLUSION

We have presented an RCS-based direct thresholding scheme for fusion of through-the-wall radar images obtained from multiple locations along two sides of the structure. Results based on real data show that the fused image has the least number of false targets, and as such, provides enhanced target detection capability as compared to the individual images.

## 7. ACKNOWLEDGMENT

This work was supported in part by DARPA under contract HR0011-07-1-0001. The content of the information does not necessarily reflect the position or the policy of the Government, and no official endorsement should be inferred.

## 8. REFERENCES

- [1] S. E. Borek, "An overview of through the wall surveillance for homeland security," *Proc. 34<sup>th</sup> Applied Imagery and Pattern Recognition Workshop*, 2005.
- [2] P. Withington, H. Fluhler, and S. Nag, "Enhancing homeland security with advanced UWB sensors," *IEEE Microw. Mag.*, vol. 4, no.3, pp. 51-58, 2003.
- [3] F. Ahmad, Y. Zhang, M. G. Amin, "Three-Dimensional Wideband Beamforming for Imaging through a Single Wall," *IEEE Geosci. Remote Sens. Letters*, Accepted for publication.
- [4] S. Papon and R. M. Narayanan, "Multiple location SAR/ISAR image fusion for enhanced characterization of targets," *Proc. SPIE*, vol. 5788, pp. 128-139, 2005.
- [5] F. Ahmad and Moeness G. Amin, "Wideband Synthetic aperture imaging for urban sensing applications," *Journal of the Franklin Institute*, March 2008.

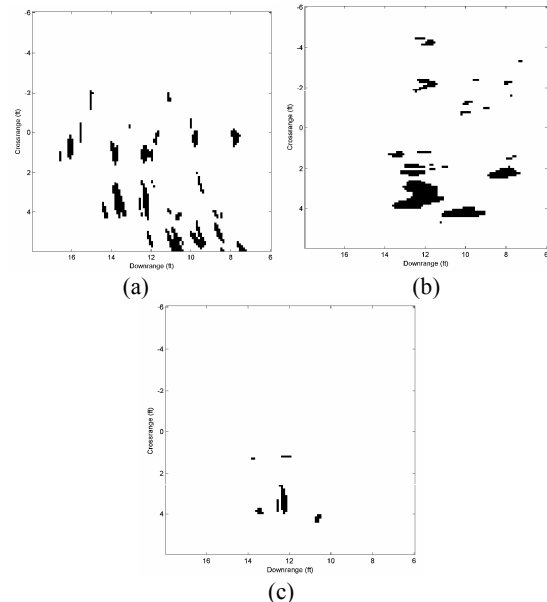


Fig. 5. Binary images (a) front wall (b) side wall.(c) fused.